VIII. PLASMA CHEMISTRY AND ION-MOLECULE INTERACTIONS

John V. Dugan, Jr.

PLASMA CHEMISTRY AND COLLISIONS

This discussion is concerned with the computation of cross sections for electron and heavy-particle collisions as well as with their plasma applications. These plasma collisions determine plasma chemistry. Electron-atom collisions and impacts of ions on molecules are of interest for plasma rate calculations. An outline of approaches and results is shown in figure VIII-1. The microscopic cross sections for such processes are required to calculate their relative probabilities. For a fixed temperature, the rate constant (or collision coefficient) is a very useful kinetic quantity. It is the Maxwell averaged product of cross section and velocity denoted by $\langle Qv \rangle$. These coefficients are used in both plasma continuity and energy equations to determine species number densities and temperatures.

Inelastic electron-atom cross sections are of particular interest since the energy transfer ΔE in these collisions is relatively large. The ΔE values range from 10 to 10^4 times the average energy loss per elastic collision. Ion-molecule collisions have large capture cross sections at thermal energies which correspond to relatively rapid chemical reactions. These reactions may be of the rearrangement type or simple charge-exchange. Both electron-atom or molecule and ion-molecule collisions control energy exchange and govern heavy particle chemistry in flowing ionized gases. Examples of such systems are an expanding hypersonic air stream and continuously operating lasers.

ELECTRON-ATOM COLLISIONS

Inelastic electron-atom collisions are important in both low ($<10^{-2}$ torr) and high pressure nonequilibrium plasmas. Elastic collisions are important only in high pressure discharges. In many cases the inelastic electron-atom cross sections have been computed using the classical Gryzinski theory. This theory is applied semiclassically with recognition of quantum structure and atomic transition

rules. Details of quantum structure are approximated in the selection of a model atom. These semiclassical cross sections have been used to calculate volume ion production costs in low pressure discharges (refs. 1 and 2). Satisfactory results of this method have been mentioned by Sovie for sustained helium plasmas. Although strictly applicable to optically thin plasmas, this approach works well for plasmas partially thick to resonance radiation. Such plasmas are found in ion engine discharges (ref. 3), radiofrequency plasma sources (ref. 4), and cathode sheaths (ref. 5).

One high pressure application of semiclassical cross sections has been in the calculation of three-body (e^- - e^- - ion) recombination rates. These rates have been computed for cesium-seeded argon (MHD application) and agree well with the experimental values (refs. 6 and 7). The semiclassical electron-atom cross sections have also been used in more elaborate plasma calculations. They are employed in calculating electronic state populations and in evaluating collision terms for the Boltzmann equation (ref. 8). This integro-differential equation is solved iteratively for the free electron distribution function $f_e(u)$, which is then used self-consistently in the rate equations for bound state populations and free electron number density N_e (ref. 9).

ION-MOLECULE COLLISIONS

Both types of ion-molecule collisions are of interest in astrophysics, astronomy, gas discharges (including masers), radiation chemistry, and molecular energetics. The early theory of Langevin considers the ion-molecule collision in terms of an ion-induced dipole interaction. This theory has been used to set upper limits to reaction cross sections for ion-molecule capture collisions. Collisions involving polar targets (i.e., molecules with permanent dipoles) cannot be treated so simply. Mass spectrometry experiments indicate that these collisions have capture cross sections larger than Langevin. Numerical capture cross sections have been calculated for these collisions (refs. 10 and 11). The shape of the ion trajectories has also been studied by means of computer-plotter techniques (refs. 12 to 14). The nature of the ion orbits raises the question of collision time so the latter was computed. Computer-plotter techniques have been recently applied to making motion pictures of ion-molecule collisions to predict chemical reactions (ref. 15).

MODEL ATOMS

Both low and high pressure rate calculations require a judicious choice of model atoms - that is, the number of discrete electronic levels considered. Two-level model atoms are satisfactory to account for excitation and ionization energy losses in volume ion production. Schematic diagrams of cesium and argon atoms are shown in figure VIII-2. It is useful to classify atoms (for eV ion^{-1} calculations) by the ratio of first excitation potential U_{ex} to ionization potential U_I (ref. 2):

$$y = \frac{U_{ex}}{U_I}$$

This parameter is equal to 0.36 for cesium (relatively easily excited low ionization potential) and 0.72 for argon (high ionization potential but easily ionized once excited). Energy losses by means of excitation to levels above the first excited state are allowed for by assigning a mean energy loss $\Delta E = (U_{ex} + U_I)/2$.

The low pressure plasmas of interest have relatively high electron temperatures from $T_e \simeq 1$ to 50 electron volts. The most detailed analyses include only ground state and metastable (long-lived) excited state populations in the rate equations. The process of stepwise excitation through upper levels leading to ionization is neglected as a source of free electrons. For the high pressure MHD plasmas, however, the excited state populations for 5 levels or so must be solved from the steady-state equations.

RESULTS

e^--Atom Cross Sections

Results of semiclassical cross-section calculations for cesium excitation and argon ionization near threshold are shown in figure VIII-3. The cesium predictions are within a factor of 2 for the first and total excitation cross sections at maximum (ref. 2). The argon ionization cross section is within several percent of experiment for 10 electron volts above threshold (ref. 2).

Electrical Conductivity

Solutions of the Boltzmann and rate equations for the free electron distribution function and state populations have been done for cesium (ref. 8). The atomic model consisted of 5 energy levels with 2- and 3-level models for comparison. The results were used to calculate electrical conductivity in cesium-seeded argon. The calculated conductivity is plotted against current density and compared with experiment in figure VII-4 (ref. 8). Comparison with elastic results (using Saha N_e values) indicates that the inclusion of the inelastic collision terms improve agreement with experiment. Results for $T_e < 2100$ K are dashed because of numerical convergence difficulties. All of the converged distribution functions are near-Maxwellian; the N_e values are with 10 percent of Maxwellian but somewhat below Saha.

Maxwellian results of ionization fraction ($f = N_e/N_0$) where N_0 is the neutral density, for 2-, 3-, and 5-level cesium model atoms are compared with detailed 26-level results in figure VIII-5. It is assumed that the plasma is optically thick to resonance radiation. The 5-level results are within factors of 2 to 5 of the 26-level results for $T_e = 0.2$ electron volt (2321 K) (ref. 9). The 5-level optically thin argon results for $T_e = 1$ electron volt (11 605 K) in figure VIII-5 show large departures of the ionization fraction from Saha. The results are also very sensitive to details of the model. This can be seen by comparison of the 2- and 3-level results with 5-level results. Plots of free electron source terms show that a step-wise ionization mechanism operates for $T_e < 2000$ K for cesium and at T_e values from 8000 K to 1 electron volt for argon.

Capture Cross Sections

Numerical solutions of the Lagrangian equations of motion have been done for capture cross sections in ion-polar molecule collisions. The coordinate system used is shown in figure VIII-6. The angle γ defines the orientation of the dipole with respect to the ion-molecule vector. The classical interaction potential has been used; it consists of ion-permanent dipole ($\mu e \cos \gamma / r^2$) and ion-induced dipole ($\alpha e^2 / 2r^4$) terms. The quantity μ is the dipole moment and α is the polarizability. Capture in Langevin collisions occurs only for impact parameters less than a critical value which is a function of α and the translational energy. Because of the dipole, the ion-polar molecule collisions are not all-or-nothing captures such as the Langevin captures. Thus, the cross section must be computed from the capture ratio C_R. This ratio is the fraction of collisions in which ion and molecule approach

within a prescribed separation for the fixed impact parameter. The variation of C_R with b^2 is shown for a typical CH_3CN-parent ion capture collision in figure VIII-7 (ref. 11). The maximum value b_m^2 for these cross sections occurs when the dipole adjusts adiabatically to the ion.

The Langevin capture ratio is also indicated in figure VIII-7. The maximum capture ratio is a step function at 425 $Å^2$. It is clear that although the dipole increases the cross section considerably above the Langevin value it does not guarantee an adiabatic collision.

The comparison of numerical and experimental cross sections as functions of maximum ion energy (corresponding to an experimental voltage setting) is made in figure VIII-8 (ref. 11). The agreement between theory and experiment is within 10 percent at all values of ion energy. Both cross sections are below the maximum.

Ion-Dipole Collision Orbits

Computer plotting techniques have been applied to the study of ion orbits in dipole collisions. The ion is reflected at separations of 1 to 3 Å to simulate the repulsive electron cores of ion and molecule. It has been proposed that long collision times due to spiraling imply large charge exchange cross sections in certain ion-molecule systems. Plots of the ion orbit for Langevin collisions demonstrate that spiraling does not occur at separations greater than 1 Å (refs. 13 and 14). However, a permanent dipole does introduce multiple reflection behavior, which leads to the formation of long-lived ion-molecule collision complexes. The multiple reflections are caused by a raising of the potential barrier due to dipole rotation. This is shown schematically in figure VIII-9.

The particles approach with relative translational energy ϵ. In the Langevin case they pass over the effective potential barrier at $r = r^*$. After reflection (at $r = r_c$), the ion simply passes out over the barrier since the maximum is fixed. In a representative ion-dipole collision the pre-reflection barrier is located at $r = r'$; however, rotation of the dipole during reflection may shift the maximum to $r = r''$ and raise it. Thus, the ion and polar molecule will reflect with efficient energy exchange until the barrier is once again lowered.

The probability of multiple reflections at impact parameters from 3 to 15 Å generally increases going from HCl to CO and CH_3CN (ref. 13). It appears that HCl has few multiple reflection collisions because of its small moment of inertia. Some CH_3CN multiple reflection cases have turning points at separations as large as 23 Å. A typical ion-orbit is shown in figure VIII-10 for a 10 reflection $CH_3CN^+ + CH_3CN$ capture collision.

The numerical cross section σ_c is independent of collision time in all cases. The values of σ_c range from Langevin ($\approx 10^2$ Å^2) for CO to 10^3 Å^2 for CH_3CN (ref. 10).

Nonpolar targets should behave like polar molecules to a greater or lesser degree. This is because their intermolecular potentials have angular dependent interaction terms. There is much evidence for long-lived complexes in such systems; for example, N_4^+ formed from impact of N_2^+ on N_2.

Computer-Made Motion Pictures

From a chemical aspect one is interested in whether the rotation of the polar molecule is hindered by the incident ion. It has been suggested that hindering will favor a specific chemical reaction. The plot of ion-dipole orientation angle as a function of ion-molecule separation is shown in figure VIII-11. These results are for a CH_3CN collision. It is clear from the γ plot (abruptly decreasing envelope) that the dipole becomes hindered at separations less than 10 Å.

Computer-made motion pictures of ion-dipole collisions allow for the simultaneous study of ion (translational) and dipole (rotational) motion (refs. 14 and 15). The sample movie frame shown in figure VIII-12 consists of ion and polar molecule models. The sum of the radii is the reflection distance r_c. There is a clock in the upper right corner consisting of a diamond moving about an asterisk. The clock speeds up and slows down since a variable step-size integration routine is used.

Movie evidence for hindered rotation in a representative collision is shown by the seven frames of figure VIII-13. Similar motion pictures of ion-dipole collisions were shown at the conference. The main features of those collisions are summarized as follows.

The first collision was a multiple reflection movie for a CO target. Three reflections occurred and the rotator was heated. The polar rotator was only slightly hindered since the μ value was relatively low (0.1 debye unit). However, the dipole played a significant enough role to cause multiple reflections.

The second collision was a HCl single reflection in which a relatively hot rotator ($E_R = 2\ kT_R$) was heated. This was an example of relatively strong interaction (dipole moment $\mu = 1.08$ debye units). The single reflection behavior was typical of HCl targets. The dipole was hindered and precessed before reflection, but rotated rather freely afterwards.

A 10 reflection CH_3CN collision was the third movie shown. The ion hindered the polar rotator so drastically that it actually became still at several different separations. In these instances the ion and polar molecule rotated about each

other to conserve total angular momentum. The CH_3CN molecule had a dipole moment of 3.92 debye units. This high μ value corresponded to an ion-dipole interaction of 3 electron volts at a typical reflection distance. This energy was about 100 times the sum of the thermal translational and rotational energies.

FUTURE PLANS

Plasma chemistry plans consist of numerical solution of the quasi-equilibrium flow of high temperature air. The ranges of temperature and pressure of interest are from thermal to 50,000 K and P/P_o from 10^{-4} to 10 (where P_o is atmospheric pressure). These values cover an interesting range for hypersonic conditions. The equilibration times for electron energy relaxation and heavy particle chemistry must be calculated to check the assumption of local thermodynamic equilibrium. Preliminary work will be done with a nitrogen model consisting of N_2, N, N_2^+, N^+, and N^{++} and e^-. Similar calculations will be done with model atoms on flowing laser systems.

A classical harmonic oscillator has been added to the ion-molecule collision model for future calculations. These ion-dipole studies will consist of computing collision lifetimes as a function of vibrational degrees of freedom. Reaction cross sections for experimental pairs will be computed from capture cross sections and hindering probabilities (γ plots).

REFERENCES

1. Sovie, Ronald J.; and Dugan, John V., Jr.: Effects of Metastable Atoms on Volume Ion Production in a Tenuous Helium Plasma. NASA TN D-3121, 1965.

2. Dugan, John V., Jr.; and Sovie, Ronald J.: Volume Ion Production Costs in Tenuous Plasmas: A General Atom Theory and Detailed Results for Helium, Argon, and Cesium. NASA TN D-4150, 1967.

3. Masek, T. D.: Plasma Properties and Performance of Mercury Ion Thrusters. Paper 69-256, AIAA, Mar. 1969.

4. Sovie, Ronald J.; and Seikel, George R.: Radio-Frequency Induction Heating of Low-Pressure Plasmas. NASA TN D-4206, 1967.

5. Nichols, L. D.; and Mantenieks, M.: Analytical and Experimental Studies of MHD Generator Cathodes Emitting in an "Spot" Mode. NASA TN D-5414 (also presented at the Annual Winter Meeting of American Society of Mechanical Engineers, Los Angeles, Calif., Nov. 16-21, 1969). Paper 69-WA/HT-51, ASME, Nov. 1969.

6. Dugan, John V., Jr.: Three-Body Collisional Recombination of Cesium Seed Ions and Electrons in High-Density Plasmas with Argon Carrier Gas. NASA TN D-2004, 1964.

7. Dugan, John V., Jr.: Calculation of Three-Body Collisional Recombination Coefficients for Cesium and Argon Atomic Ions with an Assessment of the Gryzinski Cross Sections. J. Appl. Phys., vol. 37, no. 13, Dec. 1966, pp. 5011-5012.

8. Dugan, J. V., Jr.; Lyman, F. A.; and Albers, L. U.: Solution of the Boltzmann and Rate Equations for the Electron Distribution Function and State Populations in Non-Equilibrium MHD Plasmas. Electricity from MHD. Vol. 2. International Atomic Energy Agency, 1966, pp. 85-100.

9. Dugan, John V., Jr.: The Selection of Simple Model Atoms for Calculations of Electron Density in Nonequilibrium, Low Temperature Cs Plasmas. Presented at the 27th Annual Conference for Physical Electronics, Massachusetts Inst. Tech., Cambridge, Mass., Mar. 20-22, 1967.

10. Dugan, John V., Jr.; and Magee, John L.: Capture Collisions Between Ions and Polar Molecules. J. Chem. Phys., vol. 47, no. 9, Nov. 1, 1967, pp. 3103-3113.

11. Dugan, John V., Jr.; Rice, James H.; and Magee, John L.: Calculation of Capture Cross Sections for Ion-Polar-Molecule Collisions Involving Methyl Cyanide. NASA TM X-1586, 1968.

12. Dugan, J. V., Jr.; Rice, J. H.; and Magee, J. L.: On the Nature of Ion-Molecule Collisions. Chem. Phys. Letters, vol. 2, no. 4, Aug. 1968, pp. 219-222.

13. Dugan, J. V., Jr.; Rice, J. H.; and Magee, J. L.: Evidence for Long-Lived Ion-Molecule Collision Complexes from Numerical Studies. Chem. Phys. Letters, vol. 3, no. 5, May 1969, pp. 323-326.

14. Dugan, John V., Jr.; and Rice, James H.: A Computer Plotting Description of Ion-Molecule Collisions with Long-Lived Capture Complexes. NASA TN D-5407, 1969.

15. Dugan, John V., Jr.: Canright, R. Bruce, Jr.; Palmer, Raymond W.; and Magee, John L.: Computer-Made Movies and Plotting Descriptions of Ion-Molecule Collisions with Polar Targets. Presented at Sixth International Conference on the Physics of Electronic and Atomic Collisions, Cambridge, Mass., July 28-Aug. 2, 1969.

BIBLIOGRAPHY

This bibiography comprises publications authored by the members of the NASA Lewis Research Center Staff.

Dugan, John V., Jr.: Some Theoretical Bases for Selection of Molecular Ion Propellants and a Survey of Molecular Plasma Collisions Processes. NASA TN D-1185, 1964.

Dugan, John V., Jr.: Three-Body Recombination of Cesium Ions and Electrons in an Optically Thin Plasma. Bull. Am. Phys. Soc., vol. 9, no. 3, 1964, p. 342.

Dugan, John V., Jr.: Effect of Model Atom Assumptions Upon Calculation of Electron Density in Nonequilibrium, Low-Temperature Cs Plasmas. Bull. Am. Phys. Soc., vol. 12, no. 6, Aug. 1967, p. 986.

Dugan, J. V., Jr.; and Magee, J. L.: Theory of Collisions Between Ions and Polar Molecules. Bull. Am. Phys. Soc., vol. 10, no. 2, 1965, pp. 190-191.

Dugan, John V., Jr.; and Magee, John L.: Semiclassical Approach to Capture Collisions Between Ions and Polar Molecules. NASA TN D-3229, 1966.

Dugan, John V., Jr.; and Magee, John L.: Capture Collisions between Ions and Polar Molecules. J. Chem. Phys., vol. 47, no. 9, Nov. 1, 1967, pp. 3103-3112.

Dugan, John V., Jr.; Rice, James H.; and Magee, John L.: Calculations of Capture Cross Sections for Ion-Polar Molecule Capture Collisions with CH_3CN Targets. Bull. Am. Phys. Soc., vol. 13, no. 1, Jan. 1968, p. 68.

Dugan, J. V., Jr.; Rice, J. H.; and Magee, J. L.: On the Nature of Ion-Molecule Collisions. Chem. Phys. Letters, vol. 2, no. 4, Aug. 1968, pp. 219-222.

Sheldon, John W.; and Dugan, John V., Jr.: Semiclassical Calculation of Inelastic Cross Sections for Electron-Cesium Atomic Collisions. J. Appl. Phys., vol. 36, no. 2, Feb. 1965, pp. 650-651.

Sovie, Ronald J.; and Dugan, John V., Jr.: Effects of Metastable Atoms on Volume Ion Production in a Tenuous Helium Plasma. NASA TN D-3121, 1965. Also Bull. Am. Phys. Soc., vol. 11, no. 4, 1966, p. 502.

Sovie, Ronald J.; and Dugan, John V., Jr.: Energy Required for Ion Production by Electron Bombardment in Helium, Argon, and Cesium. Bull. Am. Phys. Soc., vol. 10, no. 2, 1965, p. 179.

Sovie, R. J.; and Dugan, J. V., Jr.: Volume Ion Production Costs in Tenuous Plasma. Bull. Am. Phys. Soc., vol. 12, no. 2, Feb. 1967, p. 239.

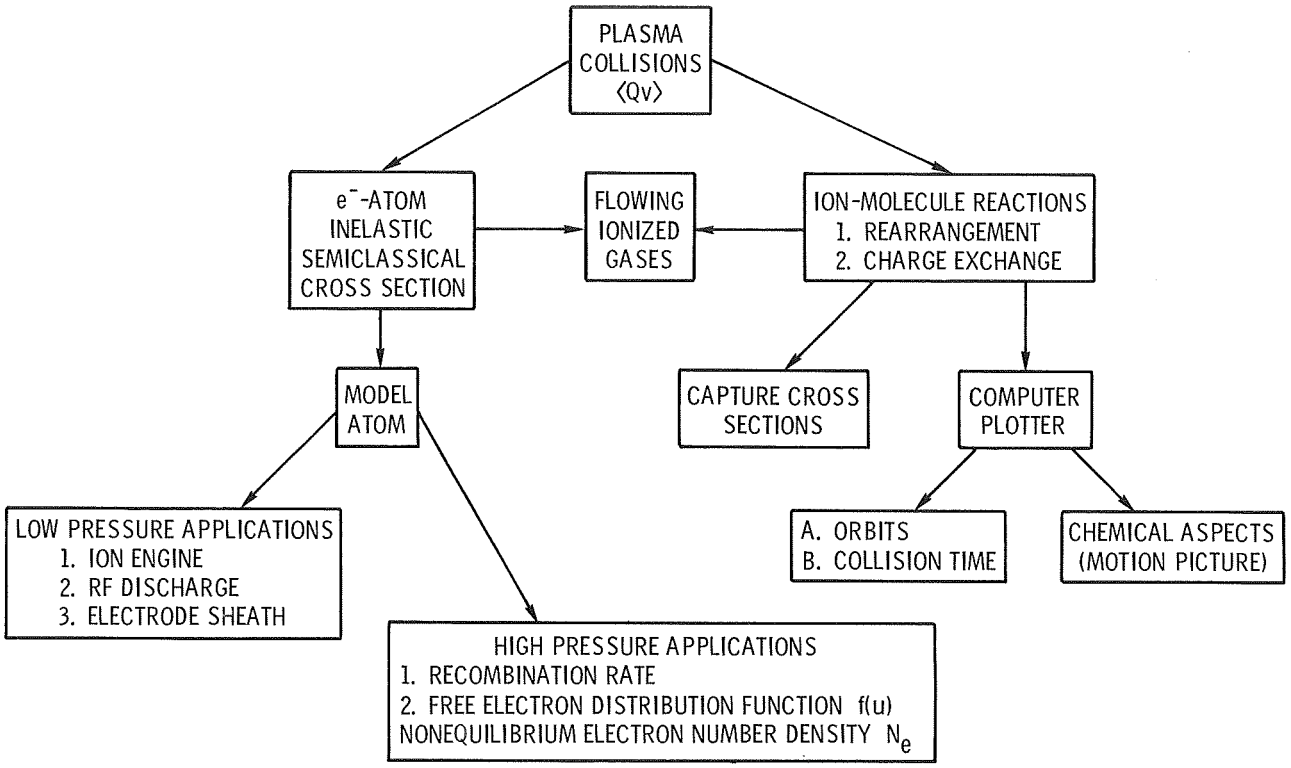

Figure VIII-1. - Outline of problems studied and approaches used in plasma chemistry and ion-molecule collisions.

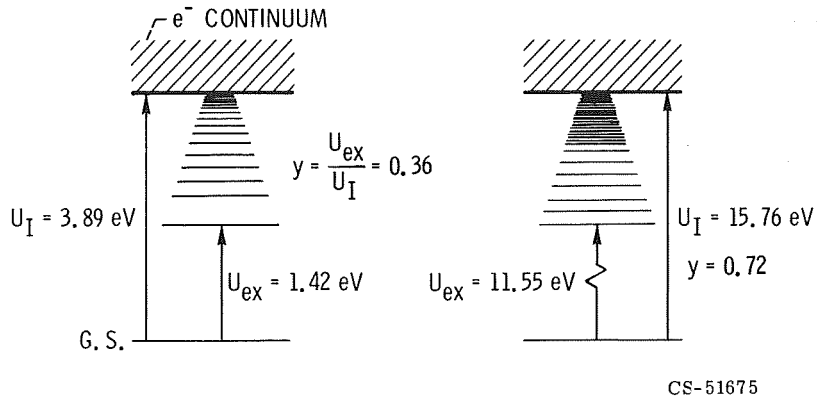

Figure VIII-2. - Schematic model atoms of cesium and argon with first excitation and ionization potentials indicated.

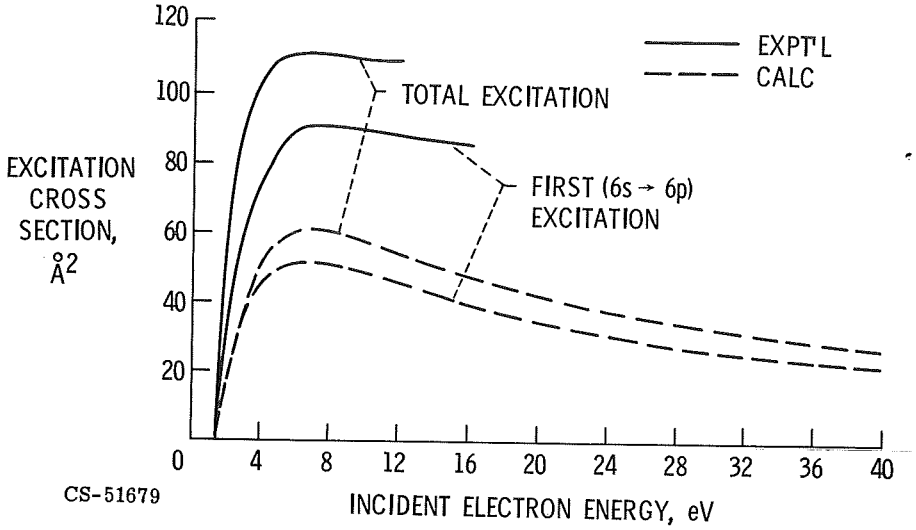

(a) Cesium excitation cross sections.

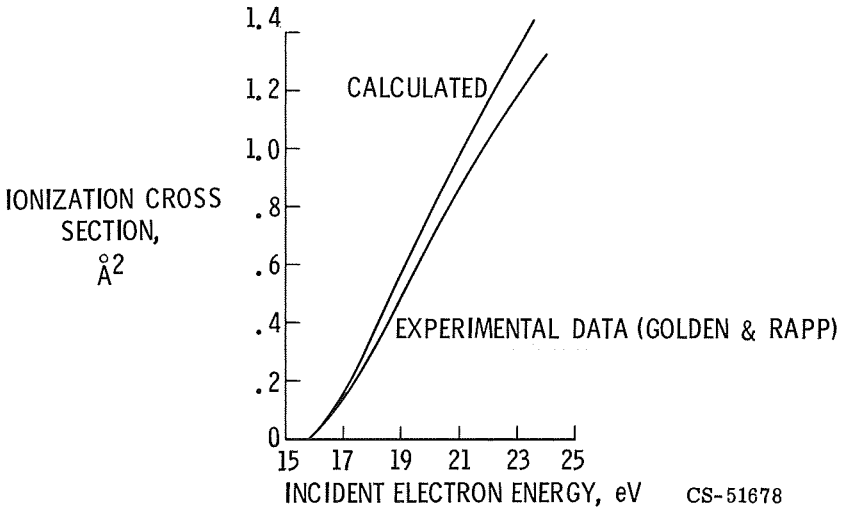

(b) Argon ionization cross section.

Figure VIII-3. - Comparison of experimental and theoretical inelastic electron-atom cross sections plotted against incident electron energy.

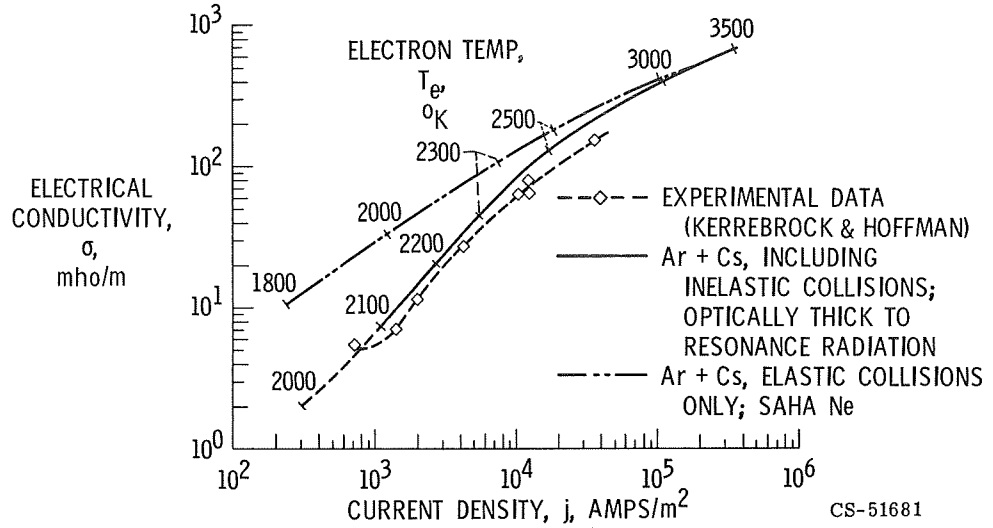

Figure VIII-4. - Comparison of experimental electrical conductivity with two sets of theoretical values for alkali-seeded argon discharges as function of current density. Atmospheric pressure; gas temperature, 1500 K; seed fraction, 0.0015.

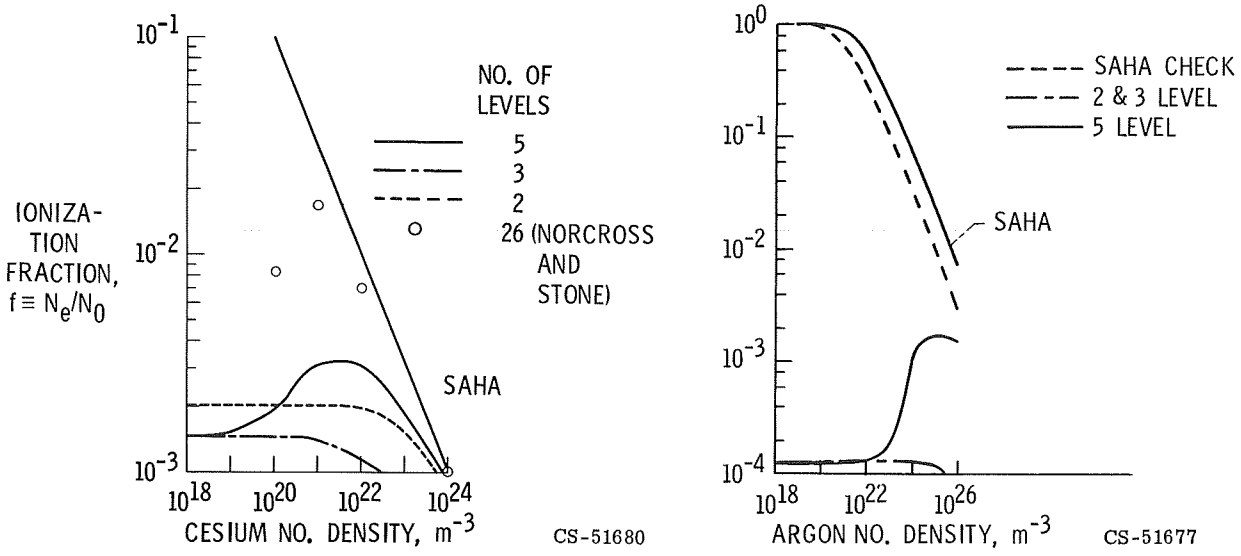

(a) Cesium. Optically thick; T_e = 2321 K (0.2 eV).

(b) Argon. Optically thin; T_e = 11 605 K (1 eV).

Figure VIII-5. - Plots of ionization fraction as function of neutral density for various model atoms.

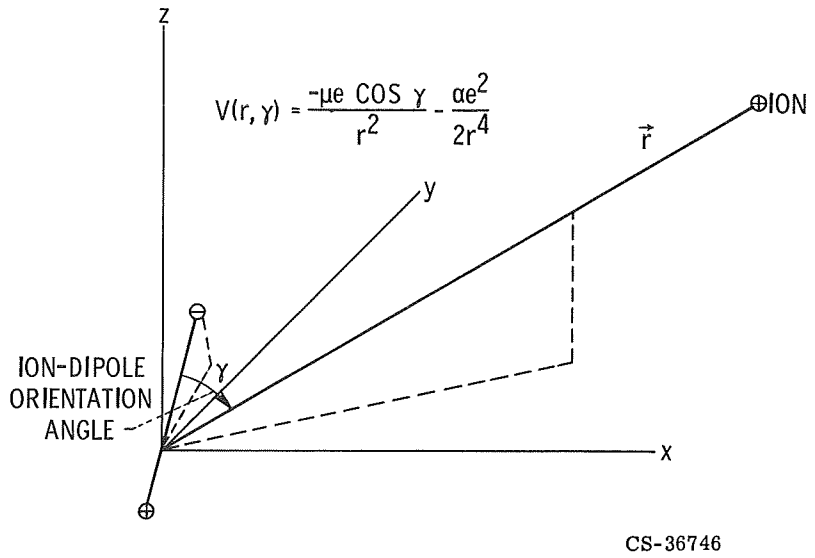

Figure VIII-6. - Coordinate system for three-dimensional interaction ion-linear molecule collision.

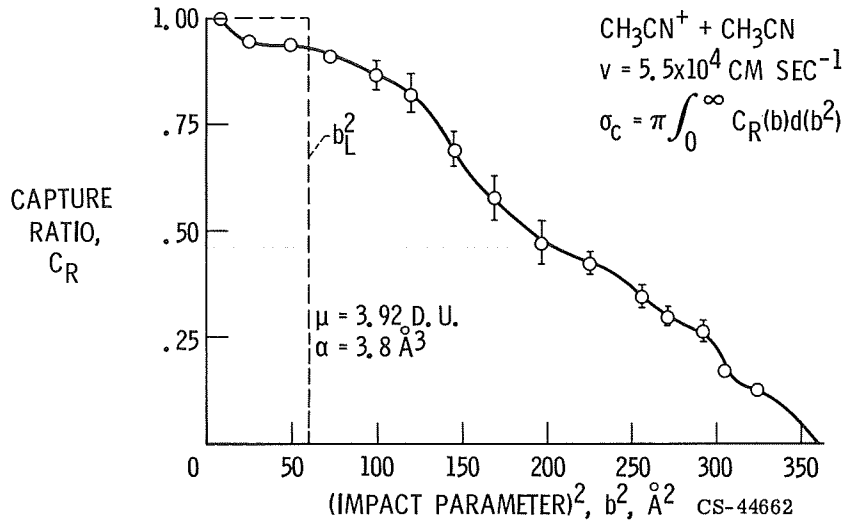

Figure VIII-7. - Variation of capture ratio (fraction of collisions for which ion and molecule approach to within 2 Å) with ion impact parameter for CH_3CN-parent ion collisions. Step-function behavior of Langevin ratio is plotted for comparison.

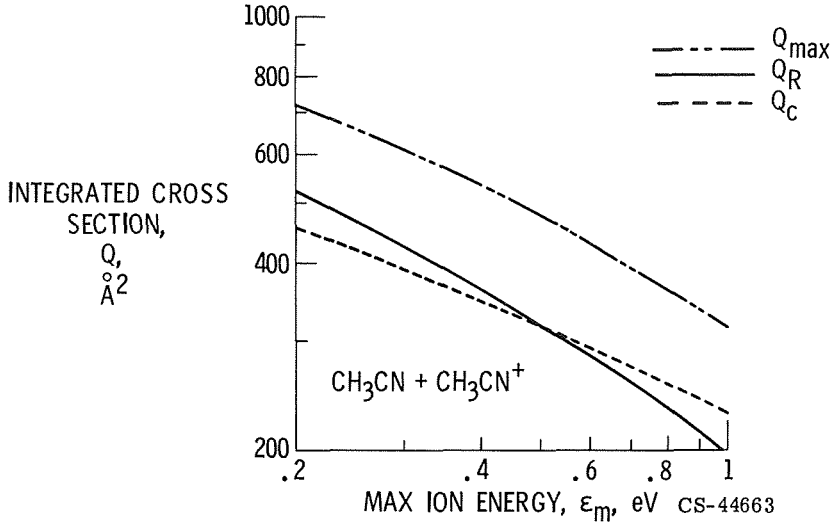

Figure VIII-8. - Maximum Q_{max}, experimental Q_R, and numerical (capture) Q_c reaction cross sections plotted against experimental voltage setting.

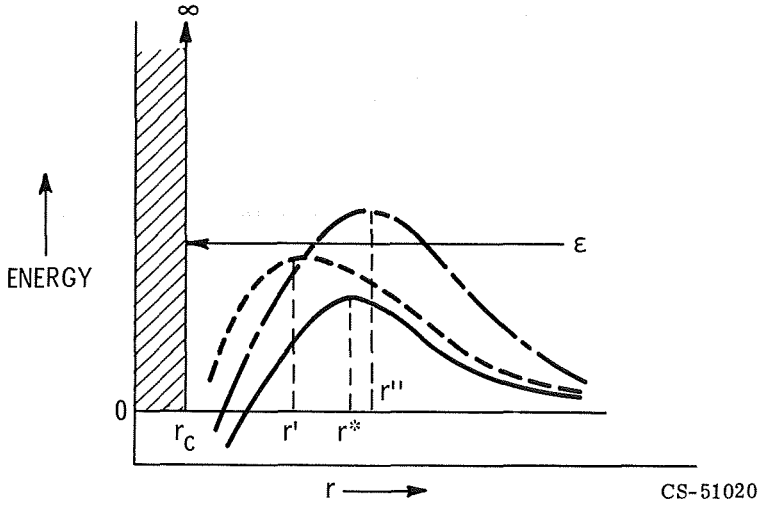

Figure VIII-9. - Schematic diagrams illustrating mechanism of multiple reflection phenomena in ion-dipole collisions with plots of effective potentials for Langevin and permanent dipole collision systems against ion-molecule separation. Ion-polar molecule interaction potential, $V_{eff}(r) = (L^2/2mr^2) + V(r)$.

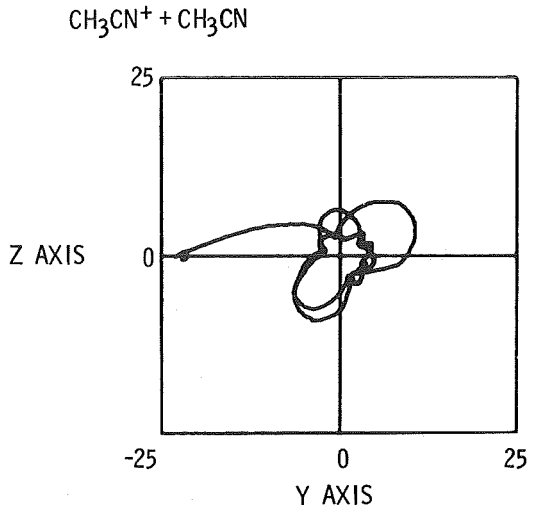

Figure VIII-10. - Trace of ion projection in Y-Z plane for 10 reflection CH_3CN-parent ion capture collision.

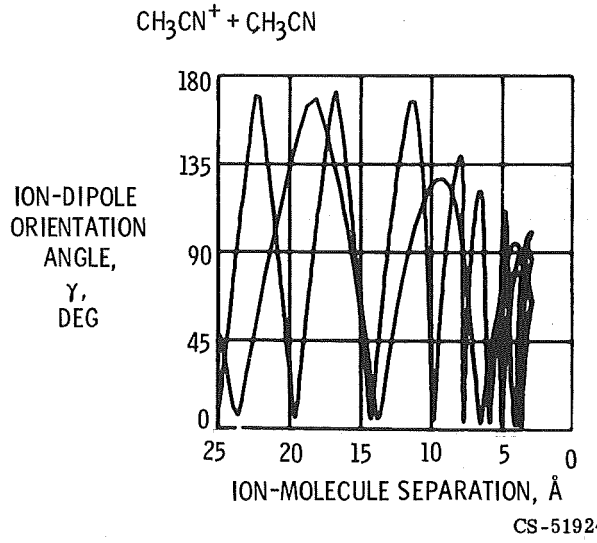

Figure VIII-11. Variation of ion-dipole orientation angle during CH_3CN-parent ion capture collision indicating hindering of the rotating dipole.

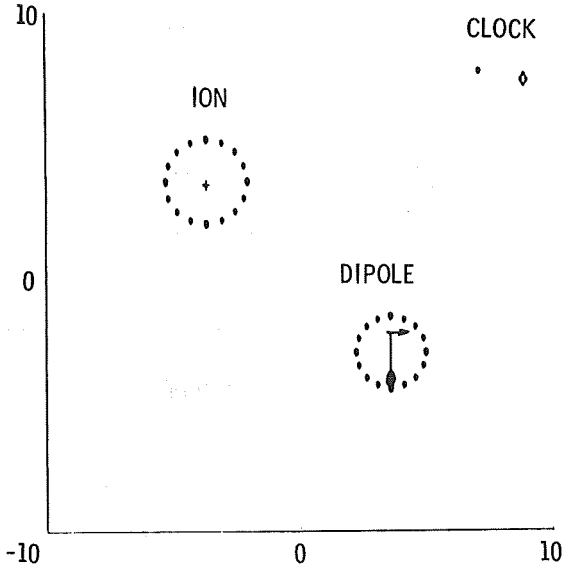

CS-51925

Figure VIII-12. - Sample motion-picture frame for CH_3CN collision.

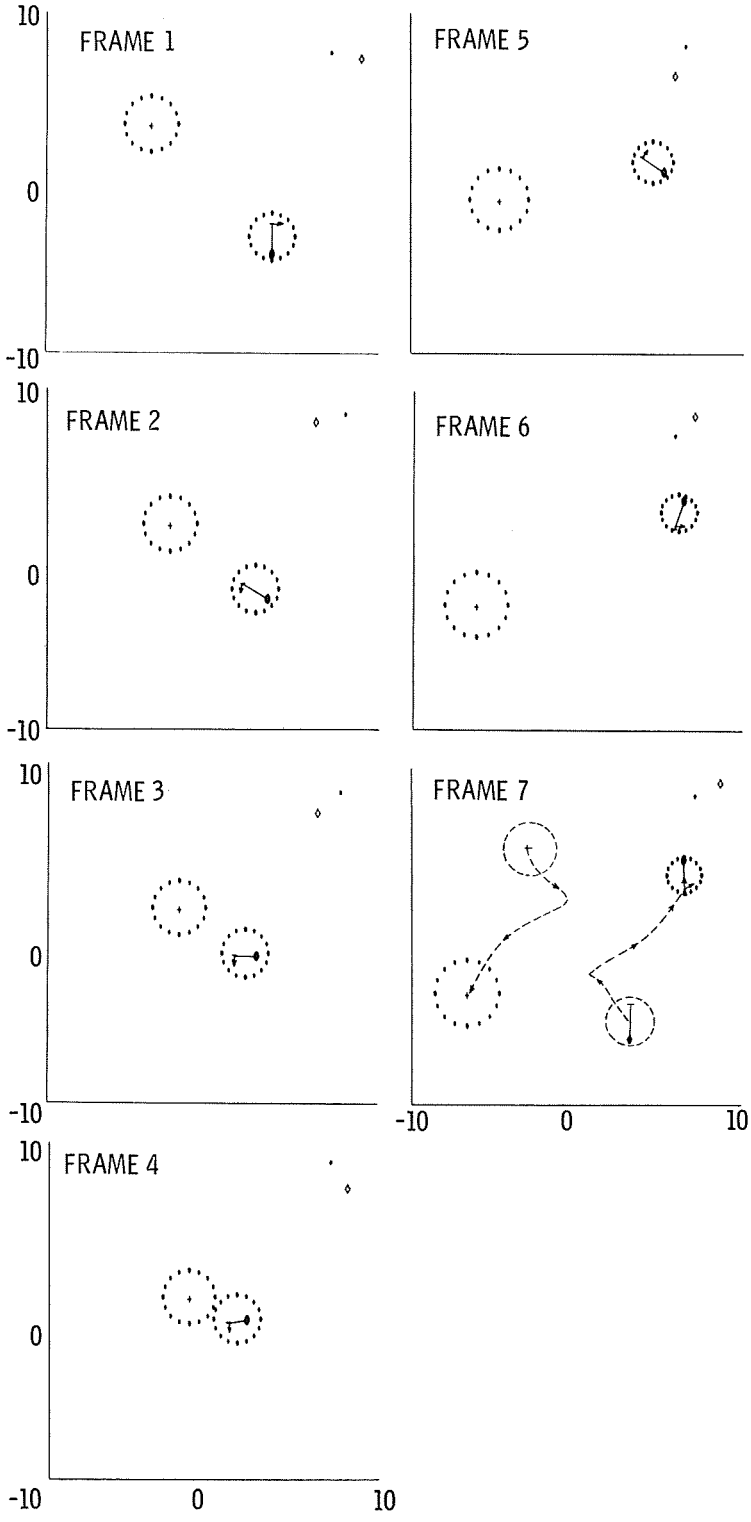

Figure VIII-13. - Motion picture evidence for hindered rotation in frames 1 to 7 for CH_3CN^+ + CH_3CN single reflection collision.